doi: 10.1111/j.1365-3121.2004.00581.x

# Movements detection of deep seated gravitational slope deformations by means of InSAR data and photogeological interpretation: northern Sicily case study

M. Saroli,[1] S. Stramondo,[2] M. Moro[2] and F. Doumaz[2]

*[1]CNR, Istituto di Geologia Ambientale e Geoingegneria, Sezione di Roma 'La Sapienza', P.le A. Moro 5, 00185 Rome; [2]Istituto Nazionale di Geofisica e Vulcanologia, Sezione di Roma, via di Vigna Murata 605, 00143 Rome, Italy*

## ABSTRACT

**We investigated the northern-central portion of Sicily region (southern Italy) using aerial photographs and Synthetic Aperture Radar (SAR) data obtained by ERS1 and ERS2 satellites. This area shows a geological-structural setting generated by the tectonic superposition of Apenninic-Maghrebian carbonatic structures on terrigenous deposits. Such a structural setting favoured the development of large-scale gravity-driven phenomena (known in the geological literature as deep-seated gravitational slope deformations) that are mostly responsible for the landscape evolution of the whole area. Morphological evidences such as landslides, sacking or rock-flow, lateral spread and block slide can be detected from photogeological analysis. In order to understand the temporal behaviour and spatial distribution of such deformations we applied the interferometric SAR (InSAR) technique. Interferograms show fringe patterns spatially coinciding with some of the large-scale gravitative phenomena previously identified by means of aerial-photo analysis. The comparison between photogeological data and InSAR results allows delimiting the active sectors in the study area.**

Terra Nova, 17, 35–43, 2005

## Introduction

Synthetic Aperture Radar (SAR) interferometry (InSAR) technique detects soil movements by calculating the satellite-to-ground distances change between two satellite acquisitions over the same area (Massonnet and Feigl, 1998). Such movements represent the superficial expression of on-going gravitational or tectonic phenomena. In this paper we propose a new InSAR application to identify movements originated by deep-seated gravitational slope deformations (DSGSD) within areas where neither seismogenic faults are identified nor significant instrumental seismic activity is recorded (Fig. 1). Preliminary results are derived from combined techniques, involving two different approaches such as aerial photographs interpretation (Volo Italia, 1988–89 flight) and SAR image analysis (ERS1–ERS2 data). The investigated area is located in the northern-central sector of Sicily (southern Italy), between the San Calogero Mt (SCM) and Pizzo Dipilo Mt (PDM)–Cervi Mt (CM), the first belonging to the Termini Imerese structure, the second to the Madonie Mountains (Fig. 2).

Correspondence: Dr Marco Moro, Istituto Nazionale di Geofisica e Vulcanologia - Sezione di Roma, via di Vigna Murata 605, 00143 Rome, Italy. Tel.: +39 06 5186 0517; fax: +39 06 5186 0507; e-mail moro@ingv.it

## Geological and structural framework

Sicily (southern Italy) is part of the western central Mediterranean region and evolves along the African–European plate boundary. Catalano *et al.* (2004), after analysing the regional facies of Mesozoic to Paleogene rocks, found that they represent the sedimentary cover of distinct palaeogeographical domains (platform/slope/basin system: Panormide, Imerese, Trapanese, Madonie domains). These domains belonged to the Tethyan Ocean and the African continental margin prior to the onset of deformation. The Miocene-Pleistocene rocks were deposited during the deformation of the mentioned domains (Catalano *et al.*, 2004).

The geological framework of northern Sicily is interpreted as resulting from recent deformations related to the opening and the evolution of the Tyrrhenian Sea, superimposed on older deformations related to the development of the Appennine–Maghrebides fold-and-thrust belt (Fig. 2) (Catalano and D'Argenio, 1982; Catalano *et al.*, 1993, 1994, 1995, 1996, 2004).

The Termini Imerese and Madonie structures represent a segment of the Maghrebide-Apenninic chain, constituted by a Meso-Cenozoic sequence and late-orogenic to post-orogenic deposits (Agnesi *et al.*, 2000a; Catalano *et al.*, 2004). The Meso-Cenozoic sequence is characterized by clay, marly and arenitic deposits belonging to the Sicilide domain (Upper Cretaceous–Lower Miocene); clay and sandstone levels of the Numidian Flysch (Upper Oligocene–Lower Miocene); carbonate deposits of the Panormide Platform (Upper Triassic–Middle Oligocene); radiolarites, siliceous claystones, calcarenites, calcirudites (Lower Cretaceous–Middle Liassic), dolomitic calcarenites and dolomitized breccias (Lower Liassic–Upper Triassic) of the Imerese Basin. Late-orogenic and post-orogenic deposits are represented by fan-delta deposits (Terravecchia Formation, Upper Tortonian–Lower Messinian) and by pelagic deposits ('Trubi' Auct., Lower Pliocene). The Imerese succession consists of Upper Triassic to Oligocene limestones, marly limestones and siliceous rocks deposited in a deep sea environment; the Panormide succession is made of Upper Triassic to Lower Oligocene – mostly shallow water carbonates. Both the Panormide and Imerese succession were covered by the Upper

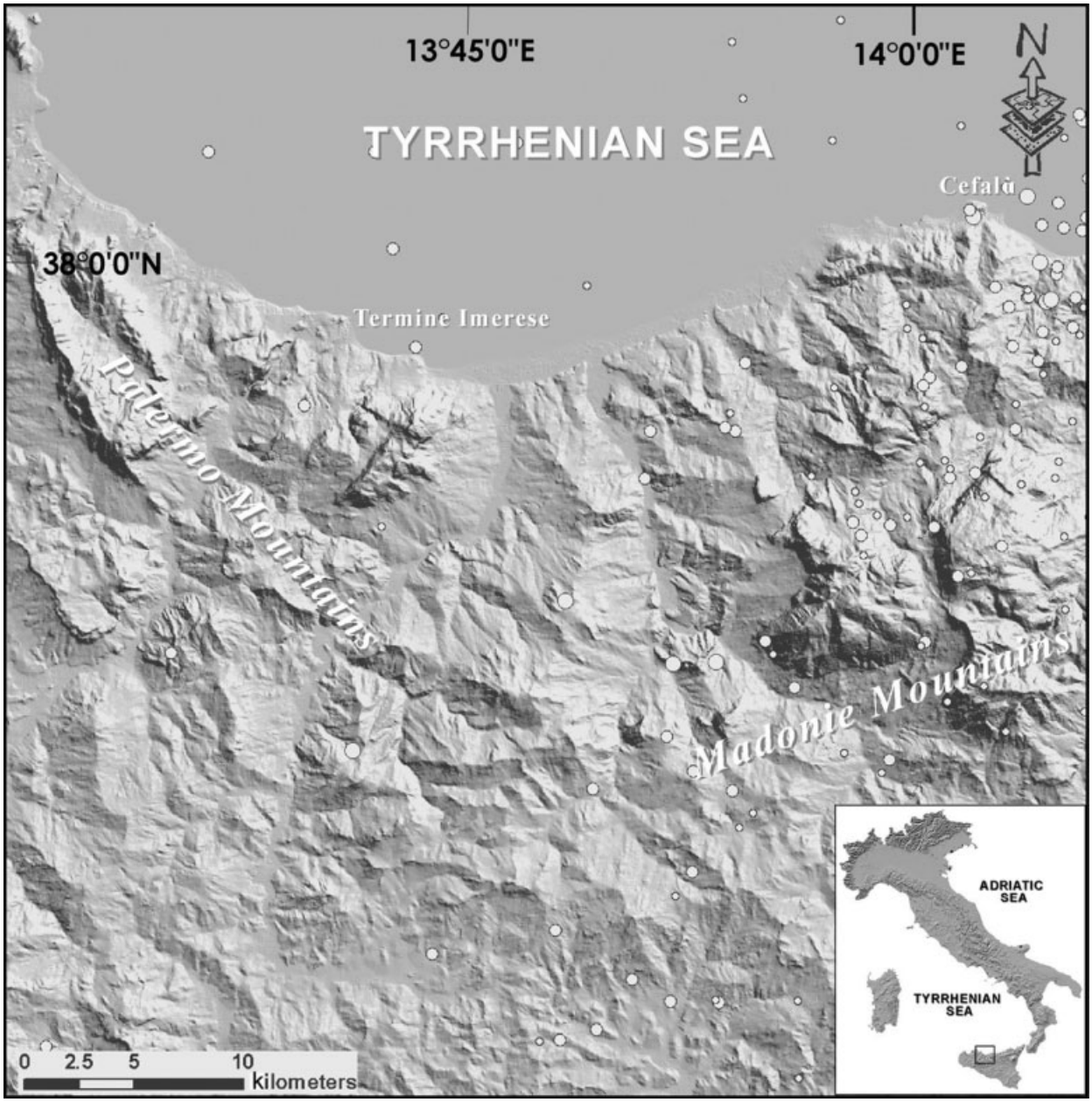


**Fig. 1** Distribution of instrumental seismicity in the study area recorded by the Istituto Nazionale di Geofisica between 1983 and 2001. White circles represent the instrumental earthquakes (1.6 < Md < 3.8).

Oligocene–Lower Miocene syntectonic Numidian Flysch.

The Termini Imerese and Madonie structures moved southwards along thrust surfaces during the construction of the Neogene Appennine–Maghrebide thrust system. Contractional deformation was accompanied by the development of coeval piggyback basin within the chain (Catalano *et al*., 1998, 2004).

The thrust-related structural framework have been overprinted by normal and strike-slip faults linked to the opening of the southern Tyrrhenian Sea that determined fault-delimited blocks rotation (Wezel, 1982; Boccaletti *et al*., 1990; Gueguen *et al*., 1997; Del Ben and Guarnieri, 2000; Catalano *et al*., 2004).

During Pliocene–Quaternary, the thrusts were accompanied by lateral movements related to right oblique transpression accompanying latest clockwise block rotations. This background produce a system of anticlinal folds dissected by reverse, normal and strike-slip faults responsible for the formation of a 'system of monoclinal faulted blocks' (Catalano *et al*., 1998, 2002, 2004; Agnesi *et al*., 2000a; Parotto and Praturlon, 2004).

Later, structural inversion of the half-graben, formed by a previous extensional event, took place during Upper Pliocene and Early Pleistocene (Lentini *et al*., 1995; Renda *et al*., 1999; Catalano *et al*., 2004). Extensional structures and compressive

 

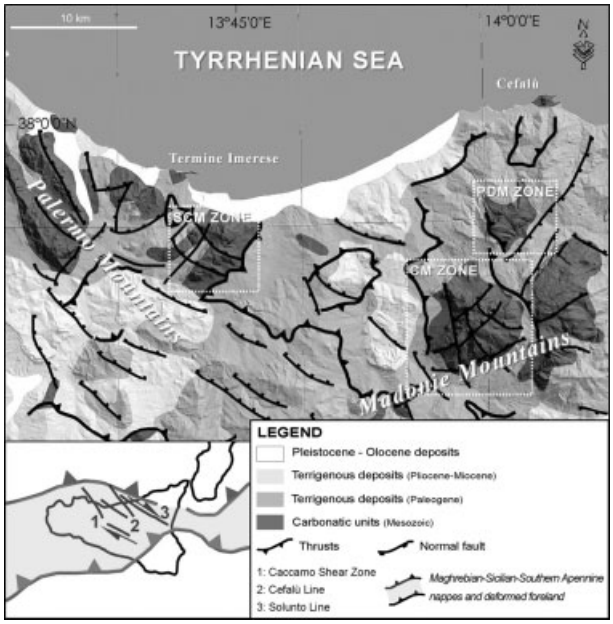


**Fig. 2** Simplified geological sketch map modified from Catalano *et al*. (2004). At the left bottom of the figure is the kinematic model of the transpressive junction. Dotted white rectangles show studied zones of San Calogero Mt (SCM zone), Pizzo Dipilo Mt (PDM zone) and Cervi Mt (CM zone).

transpressive deformation have interested the area between 1.4 and 0.5 Ma.

Vertical tectonic, imposed during the last 0.5 Myr, generate a local high relief energy; these later combined with the alternation of lithologies having different eroding degrees are responsible for the development of DSGSD processes.

## SAR interferometry results

In the last years InSAR has been successfully applied to study earthquakes, to detect and evaluate the surface displacement field (Massonnet *et al*., 1993; Stramondo *et al*., 1999); volcanoes, to estimate the pre-eruptive deflation and post-eruptive inflation (Massonnet *et al*., 1995) and landslides, to detect and monitor their temporal evolution (Fruneau *et al*., 1998; Rott *et al*., 1999). We applied InSAR to the study area using ERS1–ERS2 satellite data spanning 1999–2000. SAR images have been selected taking into account criteria such as a short orthogonal component of the spatial baseline $B_{ort}$ (i.e. the spatial baseline $B$ is the satellite-to-satellite distance while these 'look at' the same area) to reduce phase sensitivity to topography and to limit the spatial decorrelation. Moreover meteorological information from multispectral sensors ranging the VISible-Thermal InfraRed (VIS-TIR) domain have been taken into account in the SAR data selection phase. In fact, good weather conditions and constant amount of water vapour content are key points to avoid atmospheric artefacts (Zebker *et al*., 1997). To this aim we used meteorological information from Terra (MODIS sensor) and NOAA (AVHRR) satellites. MODIS is an instrument that has near-infrared (IR) channels within and around the 0.94-mm water vapour band for remote sensing of column water vapour amounts. In particular, the channels 17–18–19, at 0.905, 0.935 and 0.940 μm, are water vapour absorption channels with decreasing absorption coefficients. The strong absorption channel at 0.935 mm is most useful for dry conditions, while the weak absorption channel at 0.905 mm is most useful for very humid conditions or low solar elevation. The AVHRR has five channels in the visible, near-IR and thermal-IR (TIR) regions of spectrum. In particular, the TIR channels 4 and 5 (10.3–11.3 μm and 11.5–12.5 μm, respectively) are used to evaluate the water vapour content in atmosphere. The spatial resolution of previous data cannot detect very local atmospheric etherogeneities.

Three images from descending orbits are available: ERS1 (24 September 1999) and ERS2 (25 September 1999 and 14 October 2000).

The 25 September 1999 to 14 October 2000 differential interferogram is characterized by a very high (*c*. 4350 m) ambiguity height $h_a$ (i.e. the altitude variation corresponding to $2\pi$ phase change) that ensures the almost complete absence of topographic phase. In fact, in this sector of northern Sicily the highest relief is Mount Cervi (1475 m), which is a maximum of one-third topographic fringe in the considered interferogram. Moreover the very short orthogonal component of the spatial baseline Bort (*c*. 2 m) avoids spatial decorrelation because of the different sight angle of the two ERS images (Zebker and Villasenor, 1992). To clear the topographic contribution we used a tandem pair (i.e. 1-day temporal span) and a 20 m pixel size map-derived Digital Elevation Model (DEM). The tandem interferogram is obtained by ERS1–ERS2 24-25/09/1999 images, with an $h_a$ of *c*. 30 m. As the 25 September 1999 image is either in the tandem pair or in the differential interferogram, it allowed applying the three-pass interferometric approach. Moreover we also used the map-derived DEM to remove the topographic phase contribution. Then we preferred the map-derived DEM as it better fills holes because of the lack of coherence in some areas of the SAR tandem pair. $\sigma_{DEM}$ is the height accuracy (20 m) of the map-derived DEM, $h_a$, the ambiguity height (*c*. 4350 m for the 25 September 1999 to 14 October 2000 pair), the theoric standard deviation of the displacement measurement due to the DEM, $\sigma_{\Delta r} = \frac{\sigma_{DEM}}{h_a} \cdot \frac{\lambda}{2}$, is in this case almost negligible. The differential interferogram shows very localized fringe patterns coinciding with some of the large scale gravitative phenomena previously and independently identified through aerial-photo analysis (Fig. 3). As a result of the complex morphology of the landscape, large layover and shadowing areas are also present. The latter problems avoided a good signal in some of the selected

 

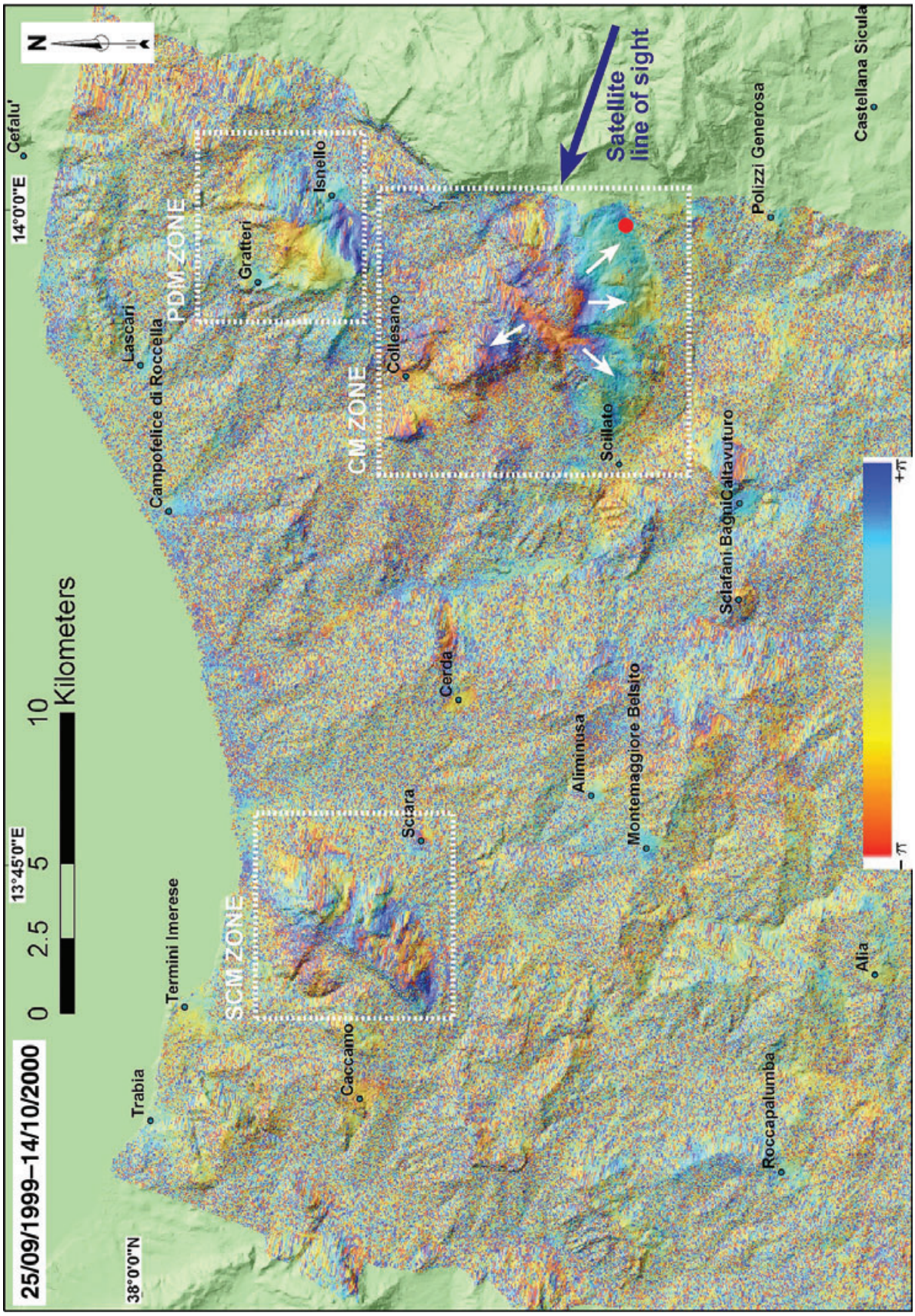


**Fig. 3** Differential interferogram spanning 25 September 1999 to 14 October 2000. Within dotted white rectangles are the three areas pointed out in Fig. 1. White arrows indicate the phase change directions and the surface movements onto the satellite line of sight. The red dot localize the selected point to propagate the phase unwrapping in Fig. 4.

areas. Only CM zone in Fig. 2 shows a clear and well-defined fringe pattern covering a square area of *c*. 6 × 6 km. White arrows indicate the direction of phase changes and the corresponding surface movements, onto the slant range direction. Each phase cycle $\pm\pi$ is equal to ≅2.8 cm (Fig. 3).

The meteorological conditions should exclude at all the presence of residual atmospheric phase contribution. On the other way, the use of a single interferogram might lead to ambiguity on the presence of artefacts, while a large amount of SAR data can adequately compensate for these artefacts (Delacourt *et al*., 1998). In particular, because of the high topographic relief of CM area, 'tropospheric fringes' (i.e. the effect of the bottom troposphere on the radar signal, producing phase changes highly correlated with the relief) could be present in the CM area.

To improve the robustness of the interpretation we unwrapped the interferogram. The solution propagates starting from a selected point in the S–E part of the CM area (Fig. 4a). Four profiles have been traced along the unwrapped phase (Fig. 4b), each one corresponding to one of the white arrows in Fig. 3, clockwise from the eastern one. Profiles follow the arrow direction. Displacements along profiles do not appear to increase with the height of the relief. Therefore a correlation of the unwrapped phase with the topography can be excluded. Consequently this confirms the interpretation of phase changes as surface displacements.

To confirm this statement, profiles point out surface movements dealing with lateral spreading of DSGSD observed in the CM area.

## Photogeological interpretation

The investigated areas (SCM, PDM and CM zones) are morphologically characterized by significant elevation changes because of the presence of high mountainous peaks, separated from surrounding depressed areas by steep escarpments. In particular, extensional faulting during Pliocene–Quaternary increased the relief energy that helped the development of gravity-driven deformations. They seem to be influenced by the inherited structural and tectonic patterns, related to the sin- and post-thrusting evolution.

Mountain slope deformation phenomena (DSGSD) are often influenced by inherited structural and geological setting; in particular, tectonic discontinuities have often turned out to be an important constraint for their onset and development (Dramis, 1984; Varnes *et al*., 1989; Dramis and Sorriso-Valvo, 1994; Thompson *et al*., 1997; Agnesi *et al*., 2000a; Agliardi *et al*., 2001; Kellogg, 2001; Onida, 2001; Di Luzio *et al*., 2004a,b).

Morphological evidences have been observed along the three zones, testifying the existence of active large-scale gravity-driven processes that have contributed to the landscape evolution of the whole zone (Figs 5a,b and 6).

Aerial photographic observation evidenced geomorphological indicators related to DSGSD (Figs 5a,b and 6); they are represented by evident double crest lines, such as scarps and counterscarps, several trenches and fractures, depression alignments. The DSGSD-induced trenches together with high production rate of debris deposits, landslides, talus slope deposits, debris flow and alluvial fans have been observed along SCM, PDM and CM. The observed upper limit of DSGSD, appear in most cases close to the main faults. They are typically curviform presenting their concavity towards downhill. The DSGSD

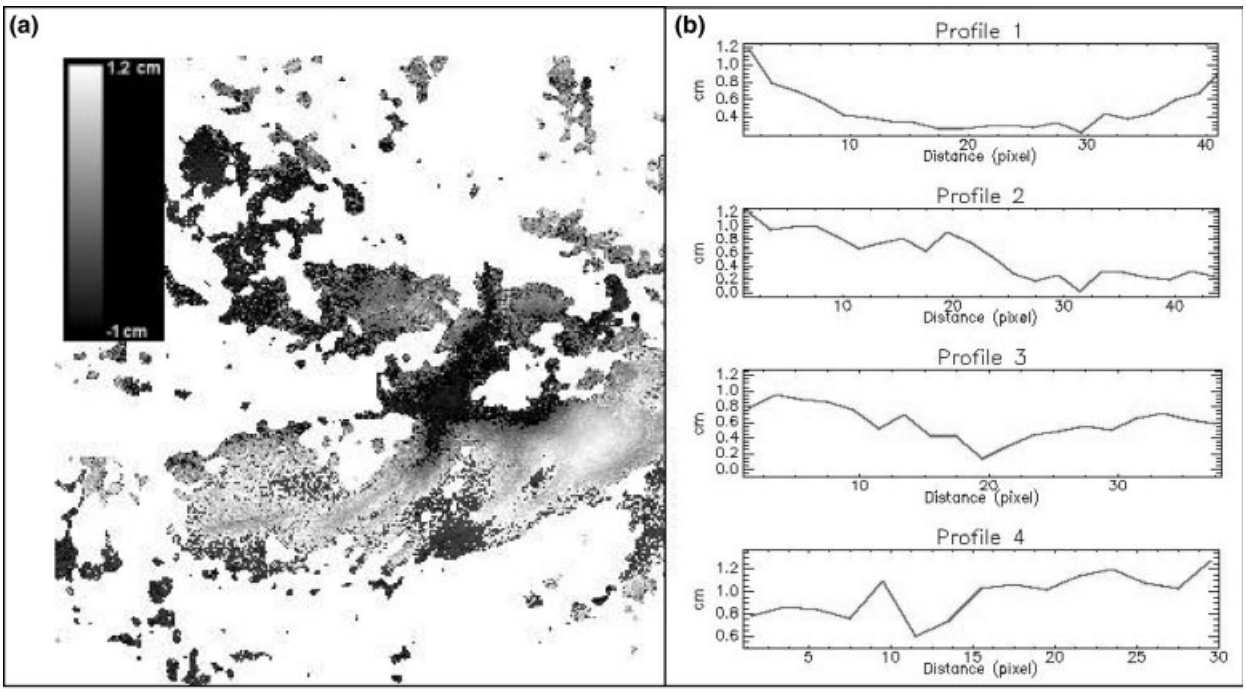


**Fig. 4** (a) Phase unwrapping of the interferogram in Fig. 3b. Displacement profiles along the unwrapped interferogram are given. The absence of a clear correlation with the relief is evident.

 

fracture patterns does not seem to be related to the main tectonic limits, because their distribution is not compatible. Hence they could be considered as mainly gravity-related features. The double crest line, clearly visible from aerial photographs and shaded relief, has been an important element in identifying DSGSD between the SCM, PDM and CM zones. Morphologic features, such as scarps and counterscarps, are also present in these zones, testifying the gravitational reactivation of DSGSD.

According to Agnesi *et al.* (2000a,b), recognized DSGSD in the CM area, using photogeological interpretation, are mainly represented by rotational sagging and lateral spreading in the central part of the structure, while the external part is mainly represented by block slides (Fig. 7). These data are confirmed by the InSAR observations that show congruent directions (radial fringes) with the type of the recognized deformation (i.e. DSGSD) (Figs 3 and 5c). In Fig. 5c,d), we present two different configurations with the same interferometric background. Figure 5c presents a scenario with DSGSD surficial expression while Fig. 5d illustrates the case with the main

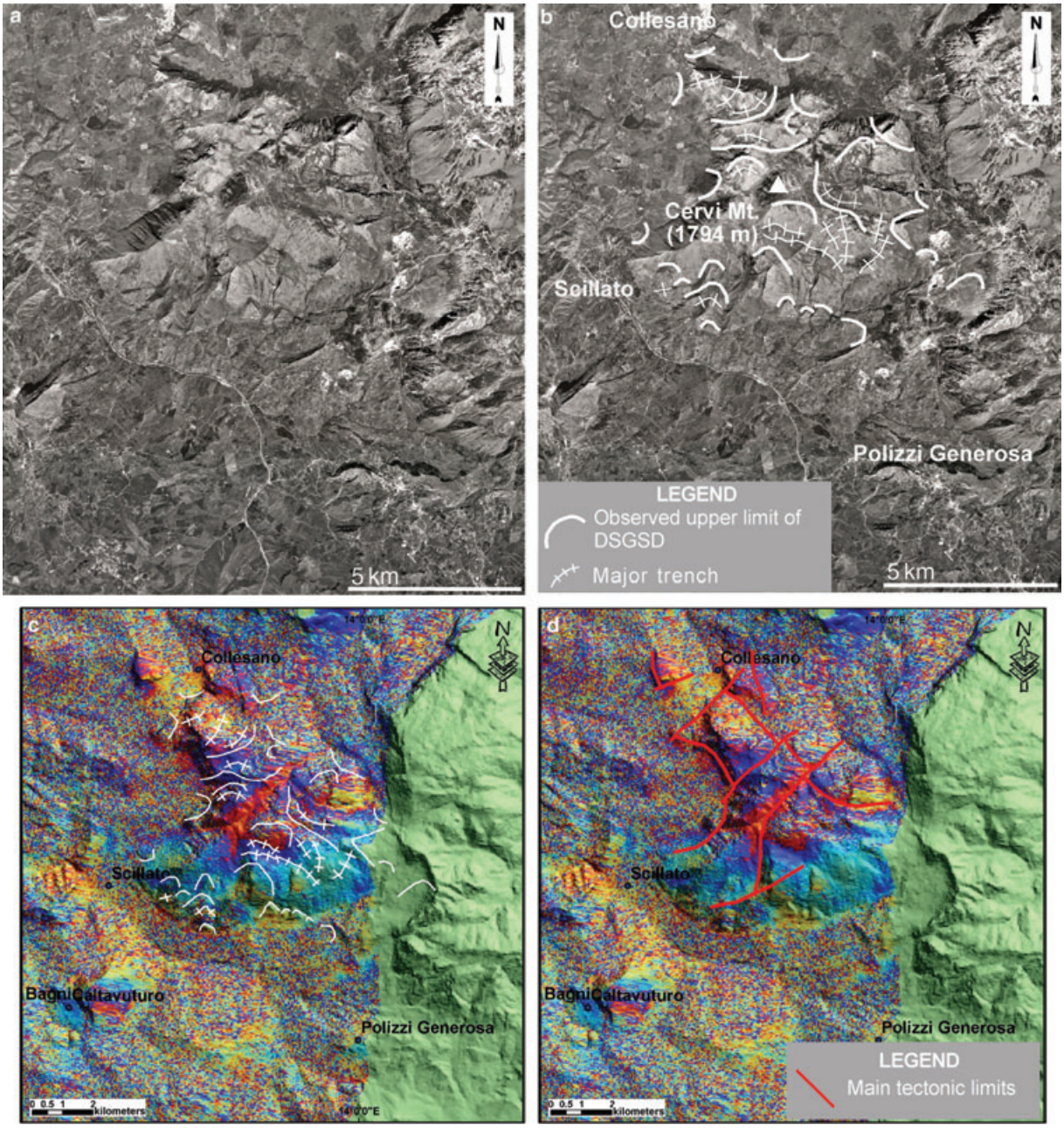


**Fig. 5** (a) Aerial photography 2062, Strip 93A, 'Volo Italia 1988–89', 1:70 000; observed features of DSGSD in the CM area from aerial photography (b) and differential interferogram; (c) main tectonic limits (modified from Agnesi *et al.*, 2000b) on differential interferogram. The deformation pattern obtained from ERS1-ERS2 image analysis, fits with the DSGSD surficial expression.

tectonic limits. The radial-like fringes distribution seems to fit better with the DSGSD surficial expression than the other expression. The case should present an abrupt change in correspondence to the main fault traces in terms of gradient (Stramondo *et al.*, 1999). A third scenario is possible if the two previous cases (gravity and tectonic) are merged but it should produce chaotic fringe patterns than radial fringes.

In two other zones of interest (SCM and PDM), InSAR shows evidences of deformation but not as the CM zone, which shows radial fringes. However, photos interpretation shows DSGSD style deformation (Fig. 6) similar to the CM zone.

Development of this specific type of DSGSD is because of the particular geological–structural setting of the area, associated with the alternation of lithologies presenting different eroding degree and a high relief energy.

Evolution of DSGSD is a consequence of the increasing relief energy, related to selective erosion and

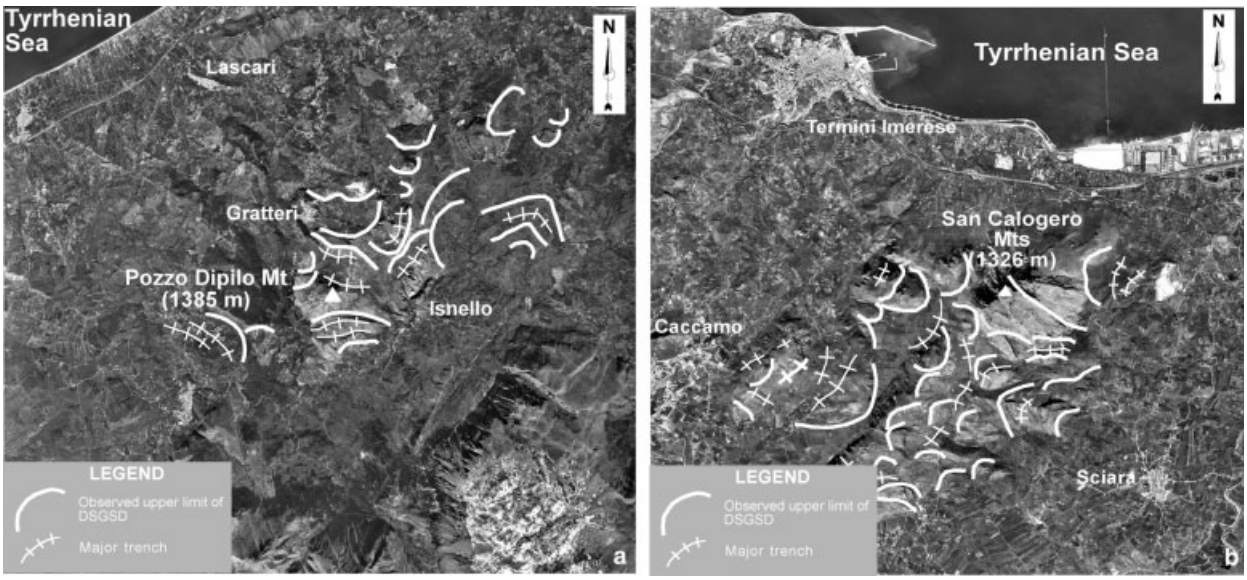


**Fig. 6** (a) Aerial photography 1120, Strip 92A, 'Volo Italia 1988–89', 1:70 000; observed features of DSGSD in the PDM area from aerial photography; (b) aerial photography 1125, Strip 92A, 'Volo Italia 1988–89', 1:70 000; observed features of DSGSD in the SCM area from aerial photography.

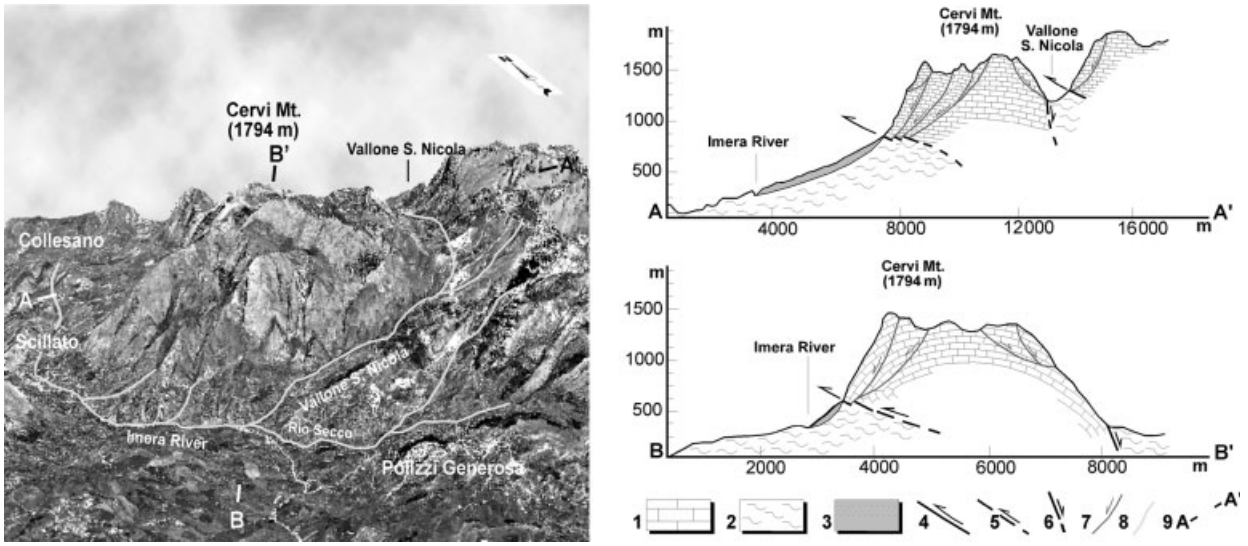


**Fig. 7** Three-dimensional view of the CM area. A-A′ and B-B′ represent simplified geological cross-sections for a DSGSD schematic interpretation. (1) Apenninic-Maghrebian carbonatic units (Meso-Cenozoic); (2) terrigenous deposits (Miocene–Pliocene); (3) debris deposits, talus slope deposits and landslides; (4) thrust; (5) inferred thrust; (6) fault; (7) principal shear surfaces reactivated by gravity; (8) drainage; (9) cross-section.

 

to the progressively deepening of the hydrographic network (Fig. 7). The variation of erosion base level can be attributed to uplift phases and eustatic oscillations, whereas tectonic events have seemingly reactivated pre-existent fault planes (Agnesi *et al*., 2000b).

## Conclusions

The InSAR results point out three localized zones (SCM, PDM and CM). In particular, the CM area is the most significant, characterized by a good coherence and showing a clear pattern of displacement fringes. In these zones photogeological interpretation allowed to identify the surficial expression of DSGSD, mainly represented by lateral spreading and sliding of carbonatic units (Agnesi *et al*., 1978, 1984, 2000a,b). On the contrary, within the considered time interval, corresponding to the InSAR time window selected images, no significant instrumental seismicity has been recorded in the study area. Hence, we exclude any eventual seismic triggered movements. Nevertheless, a seismic crisis might have a main role in emphasizing such phenomena. DSGSD might be considered the gravitative adapting to the tectonic stress variations that induced a regional or local increase of relief energy.

The deformation pattern obtained from ERS1–ERS2 image analysis seems to be clustered and not uniform on the considered area. The geometry of the ERS descending orbit, and consequently the line of sight, detected radial surface movements in CM area, as shown by the white arrows in Fig. 3. The radial-like fringes distribution fits better with the DSGSD surficial expression in comparison with the main tectonic limits as given in Fig. 5c,d.

Further studies will allow to quantify the displacement rates. The use of a large amount of SAR data and the application of InSAR time series to follow the temporal evolution of this kind of movements are foreseen. Moreover, the application of the suggested methodology to areas characterized by the presence of seismogenic faults and struck by a seismic sequence could also allow to separate tectonic and gravity contributions from the whole detected surface movement.

## Acknowledgements

At the outcome of this work, we would like to thank Francesco Guglielmino that made SAR data available. Professors A. Biasini, G. Mariotti and E. Lupia Palmieri from 'La Sapienza University' for their encouragements and advices. We thank Dr E. Carminati, for the first lecture and 'Go ahead' signal Dr F. Lenci and E. Di Luzio for corrections to the manuscript.

## References

Agliardi, F., Crosta, G. and Zanchi, A., 2001. Structural constraints on deep-seated slope deformation kinematics. *Eng. Geol*., **59**, 83–102.

Agnesi, V., Macaluso, T., Monteleone, S.G. and Pipitone, G., 1978. Espansioni laterali (Lateral Spreads) nella Sicilia occidentale. *Geol. Appl. Idrogeol*., **13**, 319–326.

Agnesi, V., Macaluso, T., Monteleone, S. and Pipitone, G., 1984. Fenomeni di deformazione gravitativa profonda (deep-seated gravitational slope deformations) osservati nella Sicilia occidentale. *Boll. Soc. Geol. It*., **103**, 671–679.

Agnesi, V., De Cristofaro, D., Di Maggio, C., Macaluso, T., Madonia, G. and Vicenza, M., 2000a. Morphotectonic setting of the Madonie area (central northern Sicily). *Mem. Soc. Geol. It*., **55**, 373–379.

Agnesi, V., Di Maggio, C., Macaluso, T. and Rotigliano, E., 2000b. Genesis and evolution of deep seated gravitational slope deformation phenomena in western and central Italy. *Mem. Soc. Geol. It*., **55**, 363–371.

Boccaletti, M., Ciaranfi, N., Casentino, D., Deiana, G., Gelati, R., Lentini, F., Massari, F., Moratti, G., Pescatore, T., Ricci Lucchi, F. and Tortrici, L., 1990. Palinspatic restoration and paleogeographic reconstruction of the peri-Thyrrenian area during the Neogene. *Palaegeogr. Palaeoclimatol. Palaeoecol*., **77**, 15–40.

Catalano, R. and D'Argenio, B., 1982. Schema geologico della Sicilia. *Soc. Geol. Ital., Guide Geol. Reg*., 9–41.

Catalano, R., Infuso, S. and Sulli, A., 1993. The pelagian foreland mad its northward foredeep. In: *Plio-Pleistocene Structural Evolution – Geological Development of the Sicilian–Tunisia platform* (M. Max and P. Colantoni, eds). *Unisco Report in Marine Science*, **58**, 37–42.

Catalano, R., Infuso, S. and Sulli, A., 1994. The submerged alpidic chain from Southern Sardinia shelf to the Pelagian rifting: tectonic history. *Boll. Geofis. Teor. Appl*., **36**, 139–158.

Catalano, R., Infuso, S. and Sulli, A., 1995. Tectonic history of the submerged Maghrebian chain from the southern Tyrrhennian sea to the pelagian foreland. *Terra Nova*, **7**, 179–188.

Catalano, R., Di Stefano, E., Vitale, F. and Sulli, A., 1996. Palaeogeography and structure of the central Mediterranean: Siculi and its offshore area. *Tectonophysics*, **260**, 5–16.

Catalano, R., Di Stefano, E., Sulli, A., Vitale, F.P., Infuso, S. and Vail, P.R., 1998. Sequence and system tracts calibrated by high-resolution biochronostrtigraphy in the central Mediterranean Plio-Pleistocene record. In: *Mesozoic and Cenozoic Sequence Stratigraphy of Europena Basins*. (P.C. Graciansky, J. Handerbol, T. Jacquin, M. Farley and P.R. Vail, eds). *SEPM Spec. Publ*., **60**, 115–177.

Catalano, R., Merlini, S. and Sulli, A., 2002. The structure of western Sicily, central Mediterranean. *Petrol. Geosci*., **8**(1), 7–18.

Catalano, R., Sulli, A., Abate, B. and Basilone, L., 2004. The crust in western and central eastern Sicily. In: *Fild Trip Guide Book – P45*, pp. 3–40. 32nd International Geological Congress. APAT, Florence, Italy.

Del Ben, A. and Guarnieri, A., 2000. Neogene transpression in the Cefalù Basin (Southern Tyrrenian): comparison between land and marine data. *Mem. Soc. Geol. It*., **55**, 27–33.

Delacourt, C., Briole, P. and Achache, J., 1998. Tropospheric corrections of SAR interferograms with strong topography: application to Etna. *Geophys. Res. Lett*., **25**, 2849–2852.

Di Luzio, E., Bianchi-Fasani, G., Saroli, M., Esposito, C., Cavinato, G.P. and Scarascia-Mugnozza, G., 2004a. Massive rock slope failure in the central Apennines (Italy): the case of the Campo di Giove rock avalanche. *Bull. Eng. Geol. Environ*., **63**, 1–12.

Di Luzio, E., Saroli, M., Esposito, C., Bianchi-Fasani, G., Cavinato, G.P. and Scarascia-Mugnozza, G., 2004b. The influence of inherited structural framework on deep-seated gravity deformation phenomena: the fault-bounded Maiella anticline (central Apennines, Italy). *Geomorphology*, **60**, 417–432.

Dramis, F., 1984. Aspetti geomorfologici e fattori genetici delle deformazioni gravitative profonde. *Boll. Soc. Geol. It*., **103**, 681–687.

Dramis, F. and Sorriso-Valvo, M., 1994. Deep-seated gravitational slope deformations, related landslide and tectonics. *Eng. Geol*., **38**, 231–243.

Fruneau, B., Delacourt, C. and Achache, J., 1998. *Observation and Modelling of the Saint-Etienne-de-Tinée Landslide*

 

*Using SAR Interferometry*. http://www.geo.unizh.ch/rsl/fringe96/papers/fruneau/index.html.

Gueguen, E., Doglioni, C. and Fernandez, M., 1997. On the-25 Ma geodynamic evolution of the western Mediterranean. *Tectonophysics*, **298**, 259–269.

Kellogg, K.S., 2001. Tectonic controls on a large landslide complex: Williams Fork Mountains near Dillon, Colorado. *Geomorphology*, **41**, 355–368.

Lentini, F., Carbone, S. and Catalano, S., 1995. Main structural domains of the central Mediterranean region and their Neogene tectonic evolution. *Boll. Geof. Teor. ed Appl.*, **XXXVI**, 141–144.

Massonnet, D. and Feigl, K., 1998. Radar interferometry and its application to changes in the earth's surface. *Rev. Geophys.*, **36**, 441–500.

Massonnet, D., Rossi, M., Carmona, C., Adragna, F., Peltzer, G., Feigl, K. and Rabaute, T., 1993. The displacement field of the Landers earthquake mapped by radar interferometry. *Nature*, **364**, 138–142.

Massonnet, D., Briole, P. and Arnaud, A., 1995. Deflation of Mount Etna monitored by spaceborne radar interferometry. *Nature*, **375**, 567–570.

Onida, M., 2001. Deformazioni gravitative profonde di versante: stato della conoscenza e progresso della ricerca in Italia. In: *Tettonica recente e instabilita' di versante nelle Alpi Centrali* (G. Pasquarè, ed.), pp. 35–74. CNR - Istituto per la Dinamica dei Processi Ambientali, Fondazione Cariplo, Milano, Italy.

Parotto, M. and Praturlon, A., 2004. The southern Apennine arc. In: *Geology of Italy. Special Volume of the Italian Geological Society for thr IGC 32 Florence*. (V. Crescenti, S. D'offizi, S. Merlino and L. Sacchi, eds), pp. 53–58. Società Geologica Italiana.

Renda, P., Tavarnelli, E. and Tramutoli, M., 1999. la distensione tetidea ed il suo controllo sulle strutture compressive del sistema appenninico-maghrebide: l'esempio della Madonne (Sicilia centro-settentrionale). *Boll. Soc. Geol. It.*, **118**, 179–190.

Rott, H., Scheuchl, B., Siegel, A. and Grasemann, B., 1999. Monitoring very slow slope movements by means of SAR interferometry: a case study from a mass waste above a reservoir in the Otztal Alps, Austria. *Geophys. Res. Lett.*, **26**, 1629–1632.

Stramondo, S., Tesauro, M., Briole, P., Sansosti, E., Salvi, S., Lanari, R., Anzidei, M., Baldi, P., Fornaro, G., Avallone, A., Buongiorno, M.F., Franceschetti, G. and Boschi, E., 1999. The September 26, 1997 Colfiorito, Italy, earthquakes: modeled coseismic surface displacement from SAR Interferometry and GPS. *Geophys. Res. Lett.*, **26**, 883–886.

Thompson, S.C., Clague, J.J. and Evans, S.G., 1997. Holocene activity of the Mt Currie Scarp, Coast Mountains, British Columbia, and implications for its origin. *Environ. Eng. Geosci.*, **3**, 329–348.

Varnes, D.J., Radbruch-Hall, D.H. and Savage, S.Z., 1989. Topographic and structural conditions in areas of gravitational spreading of ridges in the Western United States. *US Geol. Surv. Prof. Pap.*, **1496**, 28.

Wezel, F.C., 1982. Structural features and basin tectonics of the Tyrrennian Sea. In: *Geological Evolution of the Mediterranean Basin* (D.J. Stanfley and F.C. Wezel, eds). Springer-Verlag, New York.

Zebker, H.A. and Villasenor, J., 1992. Decorrelation in interferometric radar echoes. *IEEE Trans. Geosci. Remote Sens.*, **30**, 5.

Zebker, H.A., Rosen, P.A. and Hensley, S., 1997. Atmospheric effects in interferometric synthetic aperture radar surface deformation and topographic maps. *J. Geophys. Res.*, **102**, 7547–7563.

*Received 16 June 2004; revised version accepted 29 September 2004*

 